AIMS Mathematics, 11(1): 1449–1462.
DOI: 10.3934/math.2026061
Received: 25 August 2025
Revised: 06 December 2025
Accepted: 12 December 2025
Published: 19 January 2026

https://www.aimspress.com/journal/Math

Research article

A modified version of the finite volume scheme for numerical simulation of 1D non-ideal isentropic magnetogasdynamics

Reem Alotaibi[1], H. G. Abdelwahed[1,*], Kamel Mohamed[2] and Mahmoud A. E. Abdelrahman[3,4]

[1] Department of Physics, College of Science and Humanities, Al-Kharj, Prince Sattam bin Abdulaziz University, Al- Kharj11942, Saudi Arabia

[2] Department of Mathematics and computer sciences, Faculty of Science, New Valley University, New Valley, Egypt

[3] Department of Mathematics, College of Science, Taibah University, Madinah, Saudi Arabia

[4] Department of Mathematics, Faculty of Science, Mansoura University, 35516 Mansoura, Egypt

* **Correspondence:** Email: h.abdelwahed@psau.edu.sa.

Abstract: Magnetogasdynamics (MGD) is an interdisciplinary area of study that investigates the properties and behavior of electrically conductive gases, including plasmas and ionized fluids, when subjected to magnetic and electric fields. MGD is essential for simulating how electromagnetic fields affect electrically conducting gases, especially in flow regimes with high temperatures and speeds. This article examines a one-dimensional non-ideal isentropic magnetogasdynamic. We offer a modified version of finite volume (MVFV) method for the numerical analysis of this model. This approach represents an improved iteration of the Rusanov scheme, a widely utilized finite volume method for the numerical resolution of hyperbolic systems of conservation laws, particularly in the fields of MGD and fluid dynamics. The MVFV method is structured into two distinct phases: the predictor phase and the corrector phase. The predictor relies on the control parameter, which is responsible for the numerical diffusion of this method. The second phase reinstates the balance conservation equation. The MVFV technique's results are compared to the exact solution and the Harten–Lax–van Leer (HLL) approach in the numerical simulation. The findings validate the reliability of MGD models in effectively representing critical nonlinear phenomena and establish a foundation for forthcoming numerical simulations and experimental verification.

Keywords: conservation laws; non-ideal isentropic MGD; MVFV scheme; HLL scheme
Mathematics Subject Classification: 35L65, 35Q35, 65M08, 76N15, 76W05

1. Introduction

Hyperbolic systems of conservation laws represent a category of partial differential equations (PDEs) that illustrate the temporal evolution of physical quantities, including mass, momentum, and energy, while ensuring their conservation [1, 2]. They are found in many branches of research and engineering, particularly in the fields of elasticity, magnetogasdynamics, fluid dynamics, traffic flow, and plasma physics, among others. Many flow fields, including wave phenomena, are regulated by quasilinear hyperbolics of three coupled nonlinear equations. It is challenging to provide analytical solutions for nonlinear systems, especially with complex initial/boundary conditions. So, for analytic investigation, we must rely on certain analytical or numerical methodologies that may be effective in constructing the prospect and giving important information for our knowledge of the physical events involved [3, 4]. A numerical study of hyperbolic systems of conservation laws emphasizes the creation and assessment of computational techniques aimed at effectively solving these equations, which are commonly used to represent phenomena such as wave propagation, discontinuities, shocks, and rarefactions.

Magnetogasdynamics (MGD) is a specialized field within fluid mechanics that integrates the concepts of gas dynamics and electromagnetism. It focuses on analyzing the behavior of electrically conductive fluids, including plasmas, nuclear fusion, ionized gases, and liquid metals, when subjected to magnetic fields. In recent years, the study of MGD has garnered significant attention from both mathematical and physical perspectives, owing to its diverse applications across various fields, including astrophysics, nuclear science, industrial processing, electromagnetic propulsion, and plasma physics [5–7]. It is fundamentally the gas-dynamic equivalent of Magnetohydrodynamics (MHD), particularly relevant to compressible flows in high-temperature settings, including aerospace reentry vehicles, fusion reactors, and astrophysical jets. The precise resolution of the Riemann issue in relativistic MHD was examined by Glacomazzo and Rezzolla [8]. Singh et al. examined self-similar solutions pertaining to exponential shock waves within the context of non-ideal MGD [9]. The issue of shock waves traveling through a non-ideal gas has been addressed using similarity solutions [10]. The outcomes of MGD flow are not as favorable as those of traditional gas dynamics. This is due to the highly nonlinear and complex nature of the complete governing system for MGD. Therefore, it is essential to explore various simplified models. Assuming that the velocity and magnetic fields are orthogonal everywhere in the flow field, one of the basic important models is produced. Under this assumption, the one-dimensional MGD flow system resembles the gas dynamics system [11]. Hu and Sheng investigated the Riemann issue for one-dimensional magnetogasdynamics in Lagrangian coordinates using the characteristic analysis approach [12]. Kuila and Raja Sekhar investigated the Riemann problem for the one-dimensional non-ideal isentropic magnetogasdynamics with a transverse magnetic field [6].

This article employs the modified version of finite volume (MVFV) method to address the 1D isentropic magnetohydrodynamics (MGD) problem. This method consists of both predictor and corrector phases [13–15]. In the predictor step, a numerical diffusion control parameter is governed by Riemann invariants and limiters theory. The second step yields the equation for balance conservation. The stability analysis revealed that, depending on the control parameter, the MVFV technique can be of order 1 or 2 [13]. The numerical outcomes of the Hartman–Lax–van Leer (HLL) scheme have also been executed for the purposes of validation and comparison. The

Courant-Friedrich-Lewy stability requirements, which state that no gas beam may physically cross more than one cell gap in a single time step, define the time step size. A variety of test cases have been conducted, demonstrating that the MVFV technique is highly effective and powerful. Applications include space weather prediction, electromagnetic flow management in aerospace engineering, and plasma confinement, providing context for the findings. Our results validate the reliability of MGD models in accurately representing key nonlinear phenomena and establish a foundation for forthcoming numerical simulations and experimental verification.

This is the structure of the work presented. Section 2 presents the essential concepts related to one-dimensional isentropic MGD. In Section 3, the MVFV approach for addressing the one-dimensional non-ideal isentropic MGD is summarized. Section 4 presents the numerical test cases, comprising the numerical simulations and comparison between the HLL scheme and the exact solution. We also provide additional evidence for the numerical results obtained. We present our conclusions based on the current findings in Section 5.

2. The 1D non-ideal isentropic MGD model

Here, we consider the one-dimensional isentropic and ideally conductive dusty gas flow with a transversal magnetic field given as follows:

$$\begin{cases} \dfrac{\partial \rho}{\partial \mathtt{t}} + \dfrac{\partial(\rho \mathtt{u})}{\partial \mathtt{x}} = 0, \\ \dfrac{\partial \rho \mathtt{u}}{\partial \mathtt{t}} + \dfrac{\partial\left(\rho \mathtt{u}^2 + \mathtt{p} + \frac{\mathtt{B}^2}{2\mu}\right)}{\partial \mathtt{x}} = 0, \\ \dfrac{\partial \mathtt{B}}{\partial \mathtt{t}} + \dfrac{\partial(\mathtt{B}\mathtt{u})}{\partial \mathtt{x}} = 0, \end{cases} \tag{2.1}$$

where $\mathtt{B}$, $\mu > \mathtt{0}$, $\mathtt{u}$ and ρ denote the transverse magnetic induction, magnetic permeability, velocity, and density. In this case, $\mathtt{a}$ is the van der Waals excluded volume, and $\mathtt{p} = \mathtt{k}(\frac{\rho}{1-\mathtt{a}\rho})^{\gamma}$. Observably, the ideal gas in MGD is represented by the case $\mathtt{a} = \mathtt{0}$. In actuality, the above system (2.1) can be expressed conservatively as the following:

$$\frac{\partial \mathtt{W}}{\partial \mathtt{t}} + \frac{\partial \mathcal{F}(\mathtt{W})}{\partial \mathtt{x}} = 0, \tag{2.2}$$

where

$$\mathtt{W} = \begin{pmatrix} \rho \\ \rho \mathtt{u} \\ \mathtt{B} \end{pmatrix}, \text{ and}$$

$$\mathcal{F}(\mathtt{W}) = \begin{pmatrix} \rho \mathtt{u} \\ \rho \mathtt{u}^2 + \mathtt{p} + \frac{\mathtt{B}^2}{2} \\ \mathtt{B}\mathtt{u} \end{pmatrix}$$

for $\mu = 1$ in (2.1). For a smooth solution, we can rewrite the system (2.2) as follows:

$$\mathtt{U}_t + \mathtt{A}(\mathtt{U})\mathtt{U}_x = 0, \tag{2.3}$$

where

$$U = \begin{pmatrix} \rho \\ u \\ B \end{pmatrix}, \text{ and}$$

$$A(U) = \begin{bmatrix} u & \rho & 0 \\ \frac{k\gamma\rho^{(\gamma-2)}}{(1-a\rho)^{(\gamma+1)}} & u & \frac{B}{\rho} \\ 0 & B & u \end{bmatrix}.$$

Hence, the matrix $A(U)$'s eigenvalues can be expressed as follows:

$$\lambda_1 = u - c, \quad \lambda_2 = u \quad \text{and} \quad \lambda_3 = u + c, \tag{2.4}$$

$c = \sqrt{\frac{B^2}{\rho} + \frac{\gamma p}{\rho(1-a\rho)}}$. Because $c > 0$, $A(U)$'s eigenvalues are distinct and real.

3. MVFV method

Here, we describe the MVFV method in brief. Integrate Eq (2.2) in the domain $[t_n, t_{n+1}] \times [x_{i-\frac{1}{2}}, x_{i+\frac{1}{2}}]$, and derive the finite volume scheme, which can be expressed as the following:

$$W_i^{n+1} = W_i^n - \frac{\Delta t}{\Delta x}\left(F\left(W_{i+\frac{1}{2}}^n\right) - F\left(W_{i-\frac{1}{2}}^n\right)\right), \tag{3.1}$$

where $F(W_{i\pm\frac{1}{2}}^n)$ represents the numerical flux at the place $x = x_{i\pm\frac{1}{2}}$ in time t_n.

Generally, Riemann's solution at the cell interface $x_{i\pm\frac{1}{2}}$ is necessary for designing the numerical functions $F\left(W_{i\pm\frac{1}{2}}^n\right)$ in the finite volume the discretization process (3.1). Equation (2.2)'s self-similar solution to Riemann's problem is assumed to have the following initial condition:

$$W(x, 0) = \begin{cases} W_L, & \text{if} \quad x < 0, \\ \\ W_R, & \text{if} \quad x > 0, \end{cases} \tag{3.2}$$

is

$$W(t, x) = R_s\left(\frac{x}{t}, W_L, W_R\right),$$

and R_s represents the Riemann solution and it must be computed exactly or approximately. Thus, $W_{i\pm\frac{1}{2}}^n$ is the intermediate state in Eq (3.1) at the cell interface $x = x_{i\pm\frac{1}{2}}$ and can be written as follows:

$$W_{i+\frac{1}{2}}^n = R_s\left(0, W_i^n, W_{i+1}^n\right). \tag{3.3}$$

To create an approximation of $W_{i+\frac{1}{2}}^n$, we adjust the MVFV method; see [13, 16]. In order to build $W_{i+\frac{1}{2}}^n$, we integrate Eq (2.2) via the domain $[t_n, t_n + \theta_{i+\frac{1}{2}}^n] \times [x^-, x^+]$ that contains $x_{i+\frac{1}{2}}$. Generally, taking $x^- = x_i$ and $x^+ = x_{i+1}$ gives

$$W_{i+\frac{1}{2}}^n = \frac{\left(W_i^n + W_{i+1}^n\right)}{2} - \frac{\theta_{i+\frac{1}{2}}^n}{\Delta x}\Big(F(W_{i+1}^n) - F(W_i^n)\Big), \tag{3.4}$$

whereas the approximate average of solution $\mathtt{W}$ in $[\mathtt{t_n}, \mathtt{t_n} + \theta^{\mathtt{n}}_{\mathtt{i}+\frac{1}{2}}] \times [\mathtt{x_i}, \mathtt{x_{i+1}}]$ is denoted by $\mathtt{W}^{\mathtt{n}}_{\mathtt{i}+\frac{1}{2}}$ and written as follows:

$$\mathtt{W}^{\mathtt{n}}_{\mathtt{i}+\frac{1}{2}} = \frac{1}{\Delta \mathtt{x}} \int_{\mathtt{x}_i}^{\mathtt{x}_{i+1}} \mathtt{W}(\mathtt{x}, \mathtt{t_n} + \theta^{\mathtt{n}}_{\mathtt{i}+\frac{1}{2}}) \mathtt{dx}. \tag{3.5}$$

In order to conclude developing the MVFV method, we have chosen the variable $\theta^{\mathtt{n}}_{\mathtt{i}+1/2}$ (see [13]) as follows:

$$\theta^{\mathtt{n}}_{\mathtt{i}+\frac{1}{2}} = \alpha^{\mathtt{n}}_{\mathtt{i}+\frac{1}{2}} \frac{\Delta \mathtt{x}}{2\mathtt{S}^{\mathtt{n}}_{\mathtt{i}+\frac{1}{2}}}, \tag{3.6}$$

where the local parameter $\alpha^{\mathtt{n}}_{\mathtt{i}+\frac{1}{2}}$ needs to be computed locally, and the local Rusanov velocity, denoted by $\mathtt{S}^{\mathtt{n}}_{\mathtt{i}+\frac{1}{2}}$, is

$$\mathtt{S}^{\mathtt{n}}_{\mathtt{i}+\frac{1}{2}} = \max_{\mathtt{j}=1,\ldots,\mathtt{J}} (\max(|\, \lambda^{\mathtt{n}}_{\mathtt{j},\mathtt{i}} \,|, |\, \lambda^{\mathtt{n}}_{\mathtt{j},\mathtt{i}+1} \,|)). \tag{3.7}$$

The $\mathtt{j}$-th eigenvalues in (2.2) are represented by $\lambda^{\mathtt{n}}_{\mathtt{j},\mathtt{i}}$, so we rewrite Eq (3.4) as

$$\mathtt{W}^{\mathtt{n}}_{\mathtt{i}+\frac{1}{2}} = \frac{(\mathtt{W}^{\mathtt{n}}_{\mathtt{i}} + \mathtt{W}^{\mathtt{n}}_{\mathtt{i}+1})}{2} - \frac{\alpha^{\mathtt{n}}_{\mathtt{i}+\frac{1}{2}}}{2\mathtt{S}^{\mathtt{n}}_{\mathtt{j}+\frac{1}{2}}} \left[\mathtt{F}(\mathtt{W}^{\mathtt{n}}_{\mathtt{i}+1}) - \mathtt{F}(\mathtt{W}^{\mathtt{n}}_{\mathtt{i}})\right]. \tag{3.8}$$

From the previous equation, if we put $\alpha^{n}_{i+\frac{1}{2}} = \frac{\Delta t}{\Delta x} S^{n}_{i+\frac{1}{2}}$ the proposed scheme is equivalent to the Richtmyer scheme [17], and if we put $\alpha^{n}_{i+\frac{1}{2}} = \frac{\mathtt{S}^{\mathtt{n}}_{\mathtt{i}+\frac{1}{2}}}{\mathtt{S}^{\mathtt{n}}_{\mathtt{i}+\frac{1}{2}}}$, the suggested finite volume method is first order. Another option for the slopes $\alpha^{n}_{i+\frac{1}{2}}$ dependent on the limiter theory can be written

$$\alpha^{\mathtt{n}}_{\mathtt{i}+\frac{1}{2}} = \left(1 - \phi(\mathtt{r}_{\mathtt{i}+\frac{1}{2}})\right)\left(\alpha^{\mathtt{n}}_{\mathtt{i}+\frac{1}{2}}\right)_1 + \phi(\mathtt{r}_{\mathtt{i}+\frac{1}{2}})\left(\alpha^{\mathtt{n}}_{\mathtt{i}+\frac{1}{2}}\right)_2, \tag{3.9}$$

with

$$(\alpha^{\mathtt{n}}_{\mathtt{i}+\frac{1}{2}})_1 = \frac{\mathtt{S}^{\mathtt{n}}_{\mathtt{i}+\frac{1}{2}}}{\mathtt{s}^{\mathtt{n}}_{\mathtt{i}+\frac{1}{2}}}$$

and

$$(\alpha^{\mathtt{n}}_{\mathtt{i}+\frac{1}{2}})_2 = \frac{\Delta \mathtt{t}}{\Delta \mathtt{x}} \mathtt{S}^{\mathtt{n}}_{\mathtt{i}+\frac{1}{2}},$$

with $\mathtt{s}^{\mathtt{n}}_{\mathtt{i}+\frac{1}{2}} = \min\limits_{\mathtt{j}=1,\ldots,\mathtt{J}} (\max(|\, \lambda^{\mathtt{n}}_{\mathtt{j},\mathtt{i}} \,|, |\, \lambda^{\mathtt{n}}_{\mathtt{j},\mathtt{i}+1} \,|))$ and $\phi_{\mathtt{i}+\frac{1}{2}} = \phi\left(\mathtt{r}_{\mathtt{i}+\frac{1}{2}}\right)$ as an appropriate limiter, when a quantity is subjected to the flux limiter function ϕ. It computes the upwind changes' ratio $\mathtt{r}_{\mathtt{i}+\frac{1}{2}} = \frac{\mathtt{W}_{\mathtt{i}+1-\mathtt{q}} - \mathtt{W}_{\mathtt{i}-\mathtt{q}}}{\mathtt{W}_{\mathtt{i}+1} - \mathtt{W}_{\mathtt{i}}}$, $\mathtt{q} = \mathrm{sign}\left[\mathtt{F}'(\mathtt{W}^{\mathtt{n}}_{\mathtt{i}+\frac{1}{2}})\right]$. In conclusion, the MVFV method for Eq (2.2) is expressed as follows according to the choosing of parameter of control $\alpha^{\mathtt{n}}_{\mathtt{i}+\frac{1}{2}}$:

$$\begin{cases} \mathtt{W}^{\mathtt{n}}_{\mathtt{i}+\frac{1}{2}} = \dfrac{1}{2}(\mathtt{W}^{\mathtt{n}}_{\mathtt{i}} + \mathtt{W}^{\mathtt{n}}_{\mathtt{i}+1}) - \dfrac{\alpha^{\mathtt{n}}_{\mathtt{i}+\frac{1}{2}}}{2\mathtt{S}^{\mathtt{n}}_{\mathtt{j}+\frac{1}{2}}} \left[\mathtt{F}(\mathtt{W}^{\mathtt{n}}_{\mathtt{i}+1}) - \mathtt{F}(\mathtt{W}^{\mathtt{n}}_{\mathtt{i}})\right] \\ \mathtt{W}^{\mathtt{n}+1}_{\mathtt{i}} = \mathtt{W}^{\mathtt{n}}_{\mathtt{i}} - \mathtt{r}^{\mathtt{n}} \left[\mathtt{F}\left(\mathtt{W}^{\mathtt{n}}_{\mathtt{i}+\frac{1}{2}}\right) - \mathtt{F}\left(\mathtt{W}^{\mathtt{n}}_{\mathtt{i}-\frac{1}{2}}\right)\right]. \end{cases} \tag{3.10}$$

Proposition 3.1. *[13] Under the condition*

$$\alpha^n Mr^n \leq 1,$$

the MVFV scheme is total variation diminishing (TVD); it satisfies the maximum principle and it is L^∞ stable with

$$\alpha^n = sup_{(i\in Z)} \frac{S^n_{i+\frac{1}{2}}}{s^n_{i+\frac{1}{2}}},$$

$$M = sup \mid f'(w) \mid, w \in G,$$

and

$$G = \{w \in \mathbb{R} / \mid w \mid \leq \alpha_{\max} \parallel w_0 \parallel_{L^\infty(\mathbb{R})}\}.$$

Proposition 3.2. *The MVFV scheme is second-order under the condition*

$$\alpha^{\mathtt{n}}_{\mathtt{i}+\frac{1}{2}} = \mathtt{r}^{\mathtt{n}}_{\mathtt{i}} \mathtt{S}^{\mathtt{n}}_{\mathtt{i}+\frac{1}{2}}.$$

Based on the two previous propositions, and in order to preserve as many desirable properties as possible, we define the *MVFV* scheme in an optimal way, a strategy of local variation of the parameter $\alpha^n_{i+\frac{1}{2}}$, based on the theory of limiters, defined as follows:

$$\alpha^{\mathtt{n}}_{\mathtt{i}+\frac{1}{2}} = \left(1 - \phi(\mathtt{r}_{\mathtt{i}+\frac{1}{2}})\right)(\alpha^{\mathtt{n}}_{\mathtt{i}+\frac{1}{2}})_1 + \phi(\mathtt{r}_{\mathtt{i}+\frac{1}{2}})(\alpha^{\mathtt{n}}_{\mathtt{i}+\frac{1}{2}})_2. \tag{3.11}$$

Remark 3.1. *When $\alpha^n_{i+\frac{1}{2}} = \frac{\Delta t}{\Delta x} S^n_{i+\frac{1}{2}}$, the MVFV scheme is equivalent to the Richtmyer two-step Lax-Wendroff method [17].*

Remark 3.2. *When $\alpha^n_{i+\frac{1}{2}} = \frac{S^n_{i+\frac{1}{2}}}{s^n_{i+\frac{1}{2}}}$, the MVFV scheme is first-order [13]: From studying the truncation error of the MVFV scheme in the homogeneous linear case ($\frac{\partial u}{\partial t} + a\frac{\partial u}{\partial x} = 0$), we can write the truncation error as*

$$TE(x,t) = \frac{1}{2} ha(\mu - \alpha) u_{xx}(x,t) + O(h^2) + O(\tau^2),$$

then, the MVFV scheme is consistent of order 1 except if $\alpha = \mu$, making the scheme is consistent of order 2, with $\mu = ar = rS^n_{i+\frac{1}{2}}$.

4. The numerical results

We introduced the MVFV technique to investigate the one-dimensional, non-ideal, isentropic MGD. The fundamental components required for numerical solutions include rarefaction waves, contact discontinuities, and shock waves. Implementing the MVFV scheme and the HLL scheme, we simulate the following test problems to investigate the effectiveness of the MVFV method for numerical simulation for non-ideal, isentropic MGD of $a = 0, 0.035, 0.045$, when $a = 0$ leads to the ideal gas MGD. In all simulations, the domain of calculation $L = [-1, 1]$ is divided into a 300-grid mesh. We compare the numerical results obtained using the MVFV method, the HLL scheme, and the

exact solution. We consider the variables $\gamma = 1.4$, $k = 1$ and $\mu = 1$. The following equation illustrates the stability condition [13]:

$$\Delta t = CFL \frac{\Delta x}{\max_i \left(\left| \alpha^n_{i+\frac{1}{2}} S^n_{i+\frac{1}{2}} \right| \right)}, \tag{4.1}$$

where Eq (4.1) is used to vary the time step, and in the all test cases, we take $CFL = 0.4$.

4.1. Test case 1

We consider the following initial data [6]:

$$(\rho, u, B) = \begin{cases} (5.99924, \quad 19.5975, \quad 100.894) & if \quad x \leq 0, \\ (7.99242, \quad -6.19633, \quad 46.0950) & if \quad x > 0. \end{cases} \tag{4.2}$$

The solution of this test case includes a right shock wave, a contact discontinuity, and a left shock wave. We simulate this test case using the MVFV method with different values of $a = 0, 0.035, 0.045$ at the final time $t = 0,03s$, see the Figure 1. Also, we compare the numerical results obtained from MVFV method with those of the HLL scheme and an exact solution with the value of $a = 0$; see Figure 2.

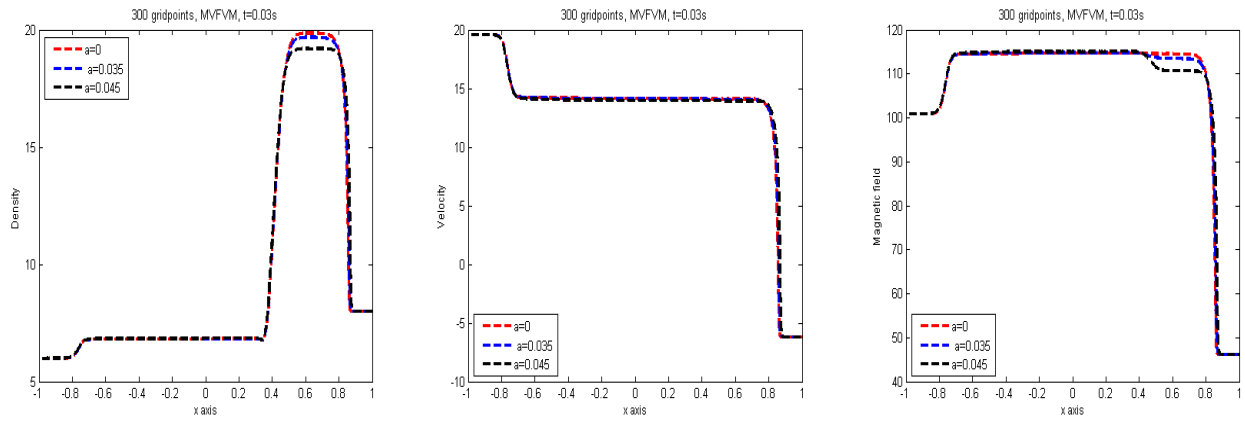

Figure 1. For various values of a, the density, velocity, magnetic field solutions at final time t = 0.03s.

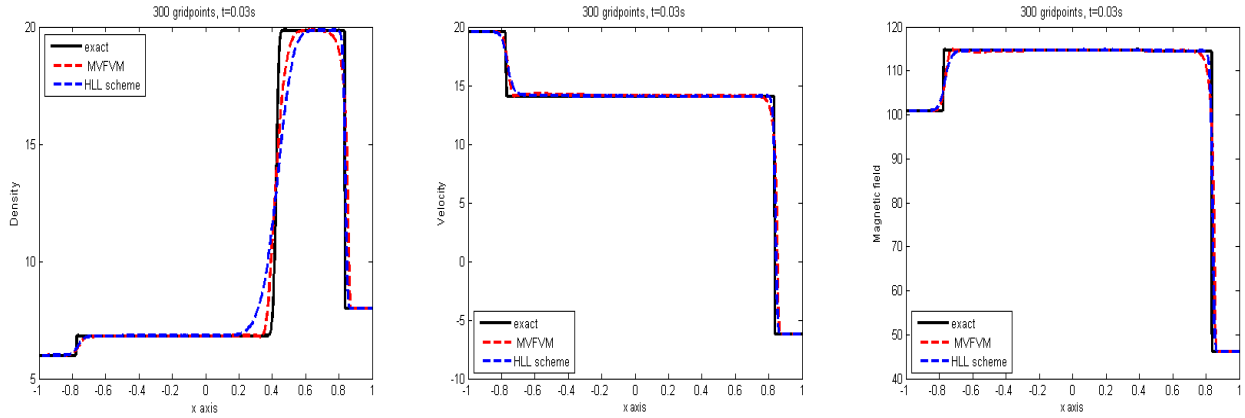

Figure 2. For value of $a = 0$, the density, velocity, magnetic field solutions at final time t = 0.03s.

4.2. Test case 2

We consider the following initial conditions [6]:

$$(\rho, \mathrm{u}, \mathrm{B}) = \begin{cases} (0.96, \quad 1.0833, \quad 2.8333) & if \quad x \leq 0, \\ (1.7741, \quad 1.1187, \quad 4.0) & if \quad x > 0. \end{cases} \tag{4.3}$$

In this case, the solution is constructed from a right rarefaction wave, a contact discontinuity, and a left shock wave. We run the MVFV method with different values of $a = 0, 0.035, 0.045$ and final time $t = 0.2s$; see Figure 3. We compare the results obtained by the MVFV method with those of the HLL scheme and exact solution with the value of $\mathtt{a} = \mathtt{0}$; see Figure 4.

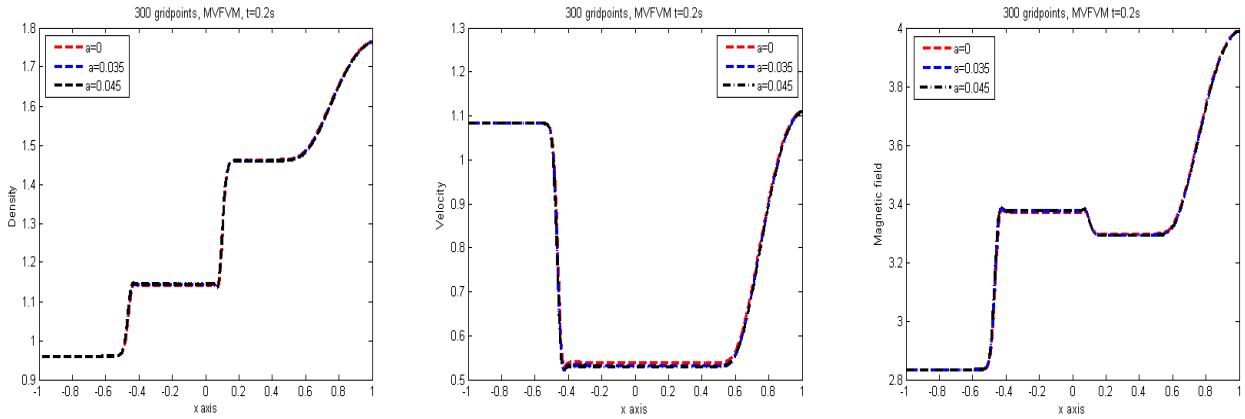

Figure 3. For various values of a, the density, velocity, magnetic field solutions at final time t = 0.2s.

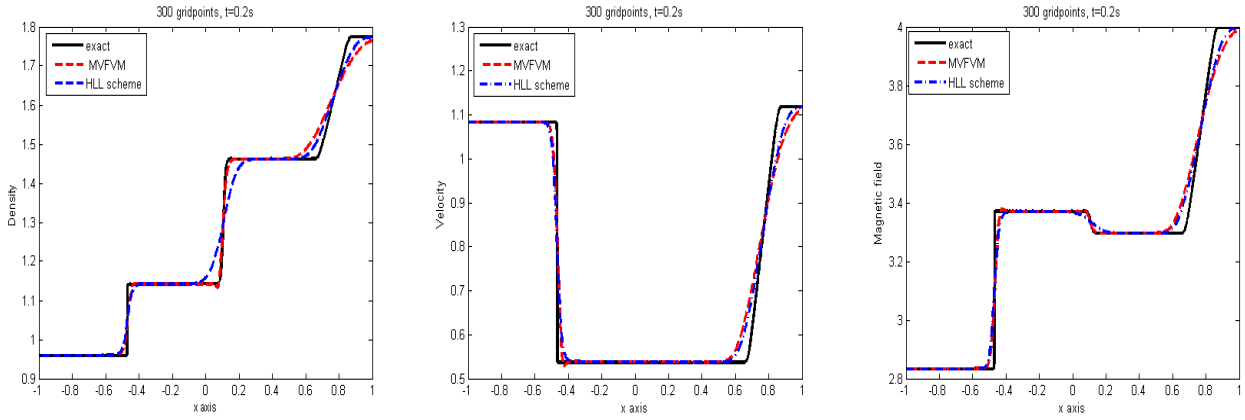

Figure 4. For value of $a = 0$, the density, velocity, magnetic field solutions at final time t = 0.2s.

In Table 1, we calculate the L_1, L_2 errors and experimental order of convergence for the two schemes. This table shows that increasing the number of gridpoints in the spatial discretization results in a decrease of L_1 and L_2 norms, and a slower decrease error in the HLL scheme than in the MVFV scheme; also, the experimental order of convergence (EOC) of the MVFV scheme is greater than that of the HLL scheme.

Table 1. The errors of L_1 and L_2 for the second test.

	MVFV				HLL			
N	L_1	EOC	L_2	EOC	L_1	EOC	L_2	EOC
50	0.0701271		0.0702295		0.0771842		0.075287	
100	0.0414846	0.746462	0.0496093	0.49422	0.051940	0.563185	0.058376	0.3617358
200	0.0239638	0.7860062	0.0330033	0.583753	0.033360	0.63413	0.044133	0.400599
400	0.0137076	0.8029744	0.0219620	0.585482	0.0210424	0.662431	0.0330129	0.41732

4.3. Test case 3

We consider the following initial conditions [6]:

$$(\rho, \mathrm{u}, \mathrm{B}) = \begin{cases} (6.0, \quad 0, \quad 1) & if \quad x \leq 0, \\ (1, \quad 0, \quad 0.1) & if \quad x > 0. \end{cases} \tag{4.4}$$

For this test case, the solution consists of a left rarefaction wave, a contact discontinuity, and a right shock wave. We apply the MVFV approach using various values of $a = 0, 0.035, 0.045$ and final time $t = 0.5s$; see Figure 5. We then compare the outcomes of the MVFV approach with those of the HLL scheme and an exact solution with the value of $\mathtt{a} = \mathtt{0}$; see Figure 6.

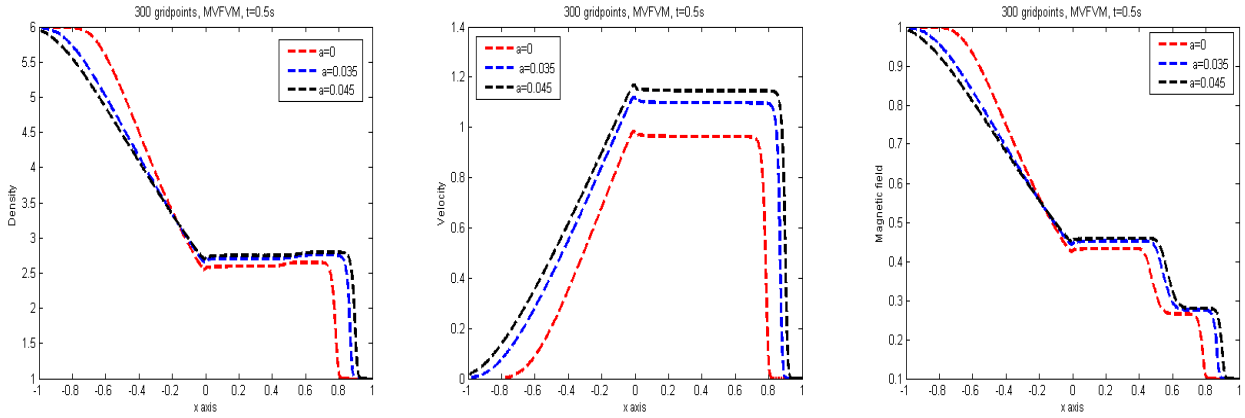

Figure 5. For various values of a, the density, velocity, magnetic field solutions at final time t = 0.5s.

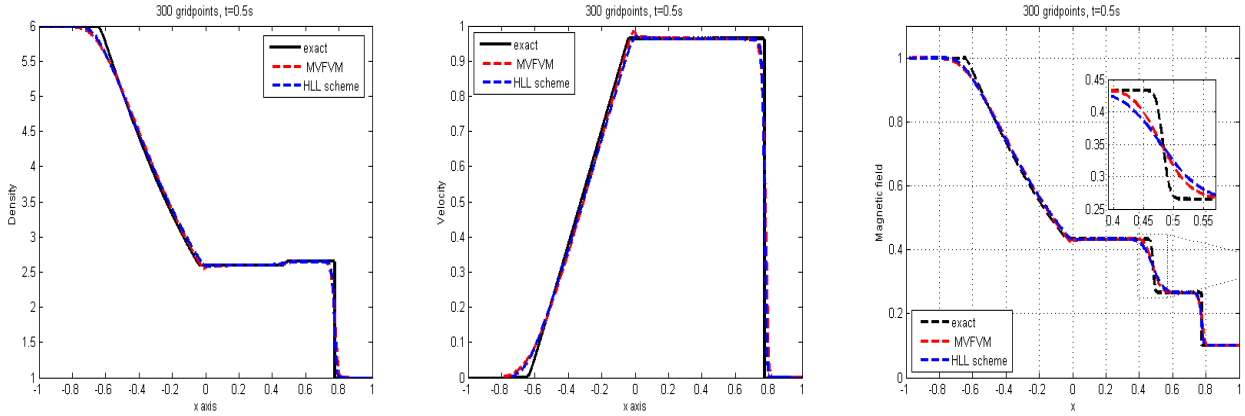

Figure 6. For value of $a = 0$, density; velocity; magnetic field solutions at final time t = 0.5s.

4.4. Test case 4

We consider the following initial conditions [6]:

$$(\rho, \mathrm{u}, \mathrm{B}) = \begin{cases} (1, \quad -0.5, \quad 0.4) & if \quad x \leq 0, \\ (1, \quad 1.5, \quad 0.4) & if \quad x > 0. \end{cases} \tag{4.5}$$

In this case, the solution is represented by a left rarefaction wave, a contact discontinuity, and a right rarefaction wave. We use different values of $a = 0, 0.035, 0.045$ and final time $t = 0.35s$ for implementing the MVFV technique; see Figure 7. We compare the numerical results obtained from the MVFV method with those of the HLL scheme and an exact solution with the value of $\mathtt{a} = \mathtt{0}$; see Figure 8.

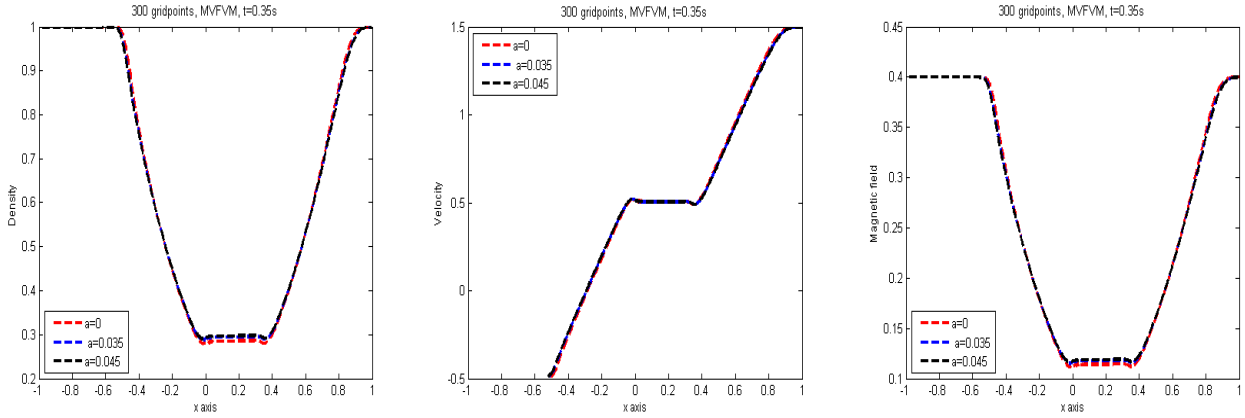

Figure 7. For various values of a, the density, velocity, magnetic field solutions at final time t = 0.35s.

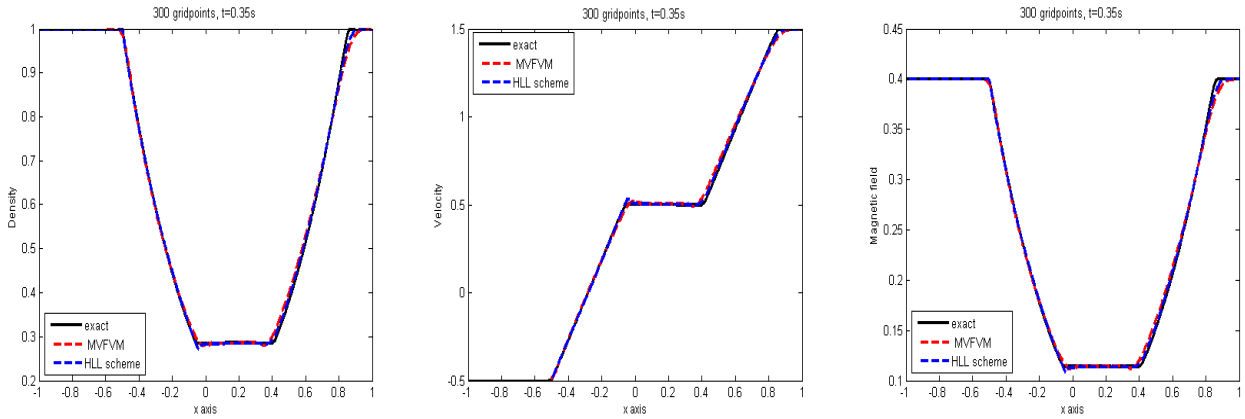

Figure 8. For value of $a = 0$, the density, velocity, magnetic field solutions at final time t = 0.35s.

To demonstrate the order of convergence of the MVFV scheme, we take the following smooth initial condition, in the domain $L = (-2\pi, 2\pi)$ at the final time $t = 0.4s$:

$$(\rho, \mathtt{u}, \mathtt{B}) = \begin{cases} (2 + sin(x), \quad 1, \quad 1) \quad if \quad x \in [-2\pi, 2\pi]. \end{cases} \tag{4.6}$$

We calculate the error L_1 in Table 2. Indeed, Figure 9 depicts the relation between $log(dx)$ and $\log(errorL_1)$, which shows that the error curve has a slope of 1.837, whereas the right side of this figure shows the behavior of the density with the exact solution.

Table 2. The error L_1 for the density.

	MVFV	
N	L_1	EOC
50	0.324122	
100	0.0996962	1.676373066
200	0.0284791	1.794591867
400	0.0076802	1.883867574
800	0.0019512	1.973217094

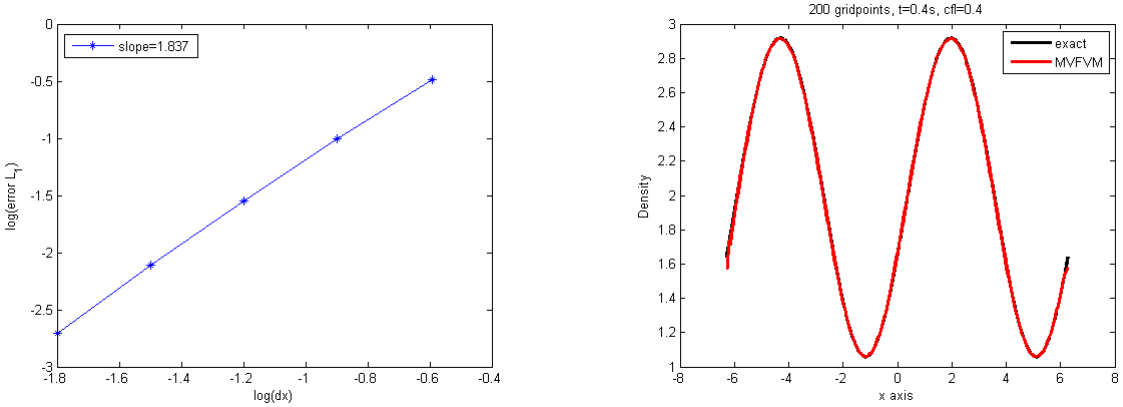

Figure 9. The relation between $log(dx)$ and $log(errorL_1)$ on the left side and the behavior of the density with the exact solution on the right side.

4.5. Computational performance

The MVFV scheme has been found to facilitate high-resolution results. As a result, the MVFV approach allows for the precise and effective numerical treatment of conservation laws. We note that the suggested MVFV scheme is in good agreement with the analytical solution and more accurate than the HLL scheme. Ultimately, the codes were developed in FORTRAN 77, and the outcomes were displayed utilizing MATLAB. These tests were conducted on a 32-bit Windows 7 machine equipped with an Intel Core i5-2520M CPU operating at 2.5 GHz.

5. Conclusions

This study utilized a modified version of a finite volume (MVFV) scheme to solve a one-dimensional, non-ideal, isentropic magnetogasdynamic in the presence of a transverse magnetic field. We also implemented the HLL scheme to compare with the proposed scheme and exact solution. The numerical findings indicate that the MVFV technique demonstrates effective resolution of shocks and rarefactions in the smooth region, achieving high accuracy. The results are framed within the context of various applications, including plasma confinement, modeling of space weather, fusion energy, and the control of electromagnetic flow in aerospace engineering.

While the current study focuses on developing and validating a finite volume scheme for numerical simulations of one-dimensional, non-ideal, isentropic magnetogasdynamic, the authors acknowledge that one-dimensional formulations have limited applicability in capturing realistic multidimensional flow structures. Future study will focus on expanding the suggested methodology to two- and three-dimensional instances, allowing for the investigation of more complex magnetogasdynamic processes and proving the method's robustness in higher dimensions.

Author contributions

Reem Alotaibi, H. G. Abdelwahed, Kamel Mohamed and Mahmoud A. E. Abdelrahman: Conception, Design, Analysis, Writing – original draft, Writing – review & editing. All authors read and approved the final manuscript.

Use of Generative-AI tools declaration

The authors declare they have not used Artificial Intelligence (AI) tools in the creation of this article.

Acknowledgments

The authors extend their appreciation to Prince Sattam bin Abdulaziz University for funding this research work through the project number (PSAU/2024/01/32064).

Conflict of interest

The authors declare that they have no competing interests.

References

1. R. J. LeVeque, *Finite volume methods for hyperbolic problems*, Cambridge: Cambridge University Press, 2002.
2. L. C. Evans, *Partial differential equations*, 2 Eds., AMS, 1998. https://doi.org/10.1090/gsm/019
3. E. F. Toro, *Riemann solvers and numerical methods for fluid dynamics*, Berlin: Springer, 1999.
4. K. Mohamed, H. A. Alkhidhr, M. A. E. Abdelrahman, The NHRS scheme for the Chaplygin gas model in one and two dimensions, *AIMS Mathematics*, **7** (2022), 17785–17801. https://doi.org/10.3934/math.2022979
5. S. Kuila, T. Raja Sekhar, Riemann solution for ideal isentropic magnetogasdynamics, *Meccanica*, **49** (2014), 2453–2465. https://doi.org/10.1007/s11012-014-0009-8
6. S. Kuila, T. Raja Sekhar, Riemann solution for one dimensional non-ideal isentropic magnetogasdynamics, *Comp. Appl. Math.*, **35** (2016), 119–133. https://doi.org/10.1007/s40314-014-0185-0
7. Y. Pang, J. Ge, H. Yang, M. Hu, The Riemann problem for an isentropic ideal dusty gas flow with a magnetic field, *Math Meth Appl Sci.*, **43** (2020), 4036–4049. https://doi.org/10.1002/mma.6172

8. B. Glacomazzo, L. Rezzolla, The exact solution of the Riemann problem in relativistic magnetohydrodynamics, *J. Fluid Mech.*, **562** (2006), 223–259. https://doi.org/10.1017/S0022112006001145
9. L. P. Singh, A. Husain, M. Singh, A self-similar solution of exponential shock waves in non-ideal magnetogasdynamics, *Meccanica*, **46** (2011), 437–445. https://doi.org/10.1007/s11012-010-9325-9
10. R. Arora, A. Tomar, V.P. Singh, Similarity solutions for strong shocks in a non-ideal gas, *Math. Model. Anal.*, **17** (2012), 351–365. https://doi.org/10.3846/13926292.2012.685957
11. R. S. Myong, P. L. Roe, Shock waves and rarefaction waves in magnetohydrodynamics part 1. A model system, *J. Plasma Phys.*, **58** (1997), 485–519. https://doi.org/10.1017/S002237789700593X
12. Y. Hu, W. Sheng, The Riemann problem of conservation laws in magnetogasdynamics, *Commun. Pure Appl. Anal.*, **12** (2013), 755–769. https://doi.org/10.3934/cpaa.2013.12.755
13. K. Mohamed, *Simulation numérique en volume finis, de problémes d'écoulements multidimensionnels raides, par un schéma de flux á deux pas*, PhD Thesis, 2005, University of Paris 13.
14. H. G. Abdelwahed, M. A. E. Abdelrahman, A. F. Alsarhana, K. Mohamed, Investigation of the Ripa model via NHRS scheme with its wide-ranging applications, *Fractal Fract.*, **6** (2022), 745. https://doi.org/10.3390/fractalfract6120745
15. K. Mohamed, Y. Omar, M. A. E. Abdelrahman, Simulating the dusty gas flow model via NHRS scheme, *Math. Meth. Appl. Sci.*, **46** (2023), 16802–16811. https://doi.org/10.1002/mma.9475
16. K. Mohamed, A finite volume method for numerical simulation of shallow water models with porosity, *Comput. Fluids.*, **104** (2014), 9–19. https://doi.org/10.1016/j.compfluid.2014.07.020
17. R. J. LeVeque, *Numerical Methods for Conservation laws*, Basel: Birkhäuser, 1992.

AIMS Press